

March 24-1950 Reider

Source of Acquisition
CASI Acquired

Copy 1
RM SL50C16a

Confidential File

CLASSIFICATION CHANGE

NACA

To Unclassified
By authority of NASA Memo 52-53
Changed by M. R. R. 6-15-73

RESEARCH MEMORANDUM

for the

Bureau of Aeronautics, Department of the Navy

THE ZERO-LIFT DRAG OF SEVERAL CONFIGURATIONS OF

THE XAAM-N-2 PILOTLESS AIRCRAFT

TED NO. NACA DE332

By James R. Hall and Carl A. Sandahl

Langley Aeronautical Laboratory
Langley Air Force Base, Va.

CLASSIFIED DOCUMENT

Restriction/Classification Cancelled

Information so classified may be imparted only to persons in the military and naval services of the United States, appropriate civilian officers and employees of the Federal Government who have a legitimate interest therein, and to United States citizens of known loyalty and discretion who of necessity must be informed thereof.

NATIONAL ADVISORY COMMITTEE
FOR AERONAUTICS

WASHINGTON

MAR 20 1950

FILE COPY
To be returned to
the files of the National
Advisory Committee
for Aeronautics
Washington, D. C.

CONFIDENTIAL

NATIONAL ADVISORY COMMITTEE FOR AERONAUTICS

RESEARCH MEMORANDUM

for the

Bureau of Aeronautics, Department of the Navy

THE ZERO-LIFT DRAG OF SEVERAL CONFIGURATIONS OF

THE XAAM-N-2 PILOTLESS AIRCRAFT

TED NO. NACA DE332

By James R. Hall and Carl A. Sandahl

SUMMARY

Free-flight tests have been made to determine the zero-lift drag of several configurations of the XAAM-N-2 pilotless aircraft. Base-pressure measurements were also obtained for some of the configurations. The results show that increasing the wing-thickness ratio from 4 to 6 percent increased the wing drag by about 100 percent at $M = 1.3$ and by about 30 percent at $M = 1.8$. Increasing the nose fineness ratio from 5.00 to 6.25 reduced the drag coefficient of the wingless models a maximum of about 0.030 (10 percent) at $M = 2.0$. A corresponding change in nose shape for the winged models decreased the drag coefficient by about 0.05 in the Mach number range from 1.1 to 1.4; at Mach numbers greater than 1.6 no measurable reduction in drag coefficient was obtained. The drag of the present Sparrow fuselage is less than that of a parabolic fuselage which could contain the same equipment.

INTRODUCTION

At the request of the Bureau of Aeronautics, Department of the Navy, an investigation of some of the aerodynamic characteristics of several configurations of the XAAM-N-2 (Sparrow) is being conducted utilizing free-flight techniques. The first phase of the investigation was concerned with the determination of the drag at zero lift of several configurations differing in nose fineness and wing-thickness ratios. This phase of the investigation has been completed and the results are reported herein. Also included are base-pressure measurements obtained for some of the configurations tested.

The flight tests were conducted at the Pilotless Aircraft Research Station at Wallops Island, Va.

SYMBOLS

C_D	drag coefficient based on maximum cross-sectional area of fuselage (0.442 sq ft)
C_{P_b}	base-pressure coefficient $\left(\frac{p_b - p_o}{q} \right)$
p_b	base pressure
p_o	ambient static pressure
q	dynamic pressure

TEST VEHICLES

The test vehicles used in this investigation were 1.125-scale models of the XAAM-N-2 pilotless aircraft. The models were constructed by the Naval Aircraft Factory at Philadelphia, Pa. The general arrangement of the models is shown in figure 1. A photograph of a typical model is shown in figure 2.

The fuselages consisted of an ogival nose section, a cylindrical center section, and a boat-tailed after section and were made of 0.064-inch-thick duralumin skin with ring stiffeners. The wings and fins were of duralumin and the wings were bolted to the fuselage center section by a single trunnion leaving a $\frac{1}{32}$ -inch gap between the wings and fuselage. Details of the wing-body intersection are given in figure 3.

In table I are listed the configurations tested. The ordinates for the two nose shapes tested are given in table II. The over-all length of the fuselages was held constant; the variation in nose fineness ratio was obtained by varying the point of tangency of the ogival nose and the center section. Model 6 was equipped with a nose telemeter antenna, dimensions of which are given in figure 4. The nose fineness ratio of this model is calculated on the basis of nose shape before being modified by installation of the antenna. All test vehicles were polished before launching.

The models were propelled by an ABL Deacon rocket motor which provided a total impulse of about 19,800 pounds-seconds over a burning period of approximately 3.5 seconds. A 5-inch HVAR booster was employed for model 5 in order to obtain data at higher Mach numbers.

Photographs of models without and with booster are shown in figures 5 and 6, respectively.

TEST METHODS

The test vehicles were tracked by Doppler velocimeter to obtain flight-path velocity and longitudinal acceleration. An SCR 584 radar set was used to obtain the flight paths. By means of standard NACA telemetry, measurements of total head, base pressure, and longitudinal and normal acceleration were obtained for several of the models.

The drag of the models was determined from values of longitudinal deceleration obtained from the Doppler velocimeter during coasting flight. These data, in conjunction with SCR 584 radar flight-path measurements, Doppler velocimeter measurements of flight-path velocity, and radiosonde observations, were used in the calculation of the total-drag coefficient as a function of Mach number. For model 6 the drag was also obtained using telemetered values of longitudinal acceleration and total head.

The base-pressure coefficient $\left(C_{Pb} = \frac{P_b - P_o}{q} \right)$ was calculated from telemetered base-pressure measurements and ambient static pressure obtained from flight path and radiosonde measurements. The flight-path velocity was obtained from telemetered total-head measurements and from Doppler velocimeter. The base-pressure pickup was located on the inside of the afterbody between the rocket nozzle and skin as shown in figure 7. The rocket nozzle and pressure pickup were insulated to eliminate thermal effects on the base-pressure pickup. The afterbody was sealed to prevent internal air flow.

Some typical flight paths, obtained with the SCR 584 radar set, are shown in figure 8. The variation of Reynolds number with Mach number for the range of altitude and climatic conditions encountered during the tests is given in figure 9.

Accuracy of Data

Drag coefficient.- The random errors in the determination of C_D , as indicated by the scatter of the data points in figure 10, are small. The systematic errors in C_D derived from Doppler velocimeter may be as large as ± 0.040 and ± 0.0075 at Mach numbers of 1.0 and 2.0, respectively. The systematic errors in C_D derived from telemeter measurements may be as large as ± 0.080 and ± 0.020 at Mach numbers 1.0 and 2.0, respectively.

Base-pressure coefficient.- The random errors in C_{pb} , as indicated by the scatter of the data points in figure 11, are small. At the lower Mach numbers investigated, these data are subject to rather high systematic errors since the quantity $p_b - p_o$ is of the same order of magnitude as the reliability of the telemetered base-pressure measurements. The systematic errors in C_{pb} may be as large as ± 0.1 and ± 0.01 at Mach numbers of 1.0 and 2.0, respectively.

RESULTS AND DISCUSSION

Drag Measurements

The variation of zero-lift drag coefficient with Mach number for the configurations tested is summarized in figure 12. The condition of zero lift was substantiated by the normal accelerometer. The results for the three wingless models agree within the accuracy of the measurements except at the highest Mach numbers investigated. The drag coefficient was reduced 0.030 (about 10 percent) at Mach number 2.0 by increasing the nose fineness ratio from 5 to 6.25. A corresponding change in nose fineness ratio for the models having wings of 4-percent-thickness ratio reduced the drag coefficient by about 0.05 in the Mach number range from 1.1 to 1.4. At the Mach numbers greater than 1.6 the change in nose fineness ratio had no measurable effect on the drag of winged models. The increase in drag due to increasing the wing-thickness ratio from 4 to 6 percent is obtained from the curves for models 2 and 3 in figure 12. The increase in wing thickness increased the wing drag (taken as the difference between the drag of the winged models and that of wingless model 6) by about 100 percent at $M = 1.3$ and by about 30 percent at $M = 1.8$. In making this comparison it is assumed that the drag of the wingless model is not affected by the presence of the nose antenna.

Base-Pressure Measurements

The variation of base-pressure coefficient with Mach number for a wingless and two winged models is given in figure 11. At the lower supersonic Mach numbers investigated, the presence of the wings tended to maintain the base-pressure coefficient at about -0.1. The base-pressure coefficient of the wingless model approached zero as the Mach number approached one. At the higher Mach numbers investigated all three configurations tended to exhibit a value of base-pressure coefficient of -0.09.

Component Drag Coefficients

The contributions of the skin-friction, base-pressure, nose-pressure, and residual-drag coefficients to the total drag coefficient measured for wingless model 6 are shown in figure 13. The residual-drag coefficient is defined here as the drag remaining after the friction, base-pressure, and nose-pressure drag coefficients have been subtracted from the total drag coefficient and consists of the fin, boat-tail pressure and fin-body interference drag coefficients. The skin-friction drag coefficient was calculated using the value of wetted-area skin-friction coefficient obtained from unpublished measurements of the boundary layer on a large-scale free-flight test vehicle. The base-pressure drag coefficient was calculated from measured values of the base-pressure coefficient obtained with model 6. The nose-pressure drag coefficient was obtained by the method of Laitone presented in reference 1.

The possibility of reducing the drag by changing the present fuselage to one of parabolic shape has been considered. A parabolic fuselage which could contain the equipment used in the actual Sparrow missile would have a maximum diameter of about 9 inches instead of 8 inches located at the 40-percent fuselage station and would taper gradually from this point to a diameter of about 6.5 inches at the base. Such a parabolic shape would have approximately the same skin-friction drag coefficient as the present shape but would have about 20 percent more nose-pressure drag. In addition, the very shallow slope of the afterbody of such a parabolic fuselage, according to unpublished work on the effect of afterbody shape on base pressure, would induce more base suction. On the basis of these considerations, it may be concluded that the fuselage tested is a good one from the standpoint of both low drag and ease of manufacture.

CONCLUSIONS

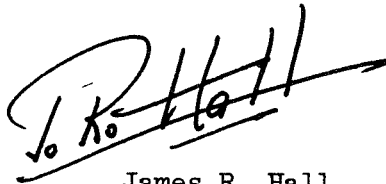
The following conclusions are based on the tests of 1.125-scale models of the XAAM-N-2 pilotless aircraft:

1. Increasing the wing-thickness ratio from 4 to 6 percent increased the wing drag by about 100 percent at $M = 1.3$ and by about 30 percent at $M = 1.8$.
2. Increasing the nose fineness ratio from 5.00 to 6.25 decreased the drag coefficient of the wingless models a maximum of about 0.030 (10 percent) at $M = 2.0$.

3. A corresponding change in nose shape for the winged models decreased the drag coefficient by about 0.05 in the Mach number range from 1.1 to 1.4. At Mach numbers greater than 1.6, no measurable reduction in drag coefficient was obtained.

4. The present fuselage has less drag than a parabolic fuselage which could contain the same equipment.

Langley Aeronautical Laboratory
National Advisory Committee for Aeronautics
Langley Air Force Base, Va.



James R. Hall
Aeronautical Research Scientist



Carl A. Sandahl
Aeronautical Aerodynamics Scientist

Approved:



Robert R. Gilruth
Chief of Pilotless Aircraft Research Division

DLMcC

REFERENCE

1. Laitone, E. V.: The Linearized Subsonic and Supersonic Flow about Inclined Slender Bodies of Revolution. Jour. Aero. Sci., vol. 14, no. 11, Nov. 1947, pp. 631-642.

TABLE I

SUMMARY OF CONFIGURATIONS TESTED

Model	Nose fineness ratio	Wing-thickness ratio (percent)	Center of gravity, fuselage station	
			Take-off	Rocket expended
1	5.00	4.0	73.7	67.7
2	6.25	4.0	76.0	70.5
3	6.25	6.0	76.5	70.5
4	5.00	Wingless	75.5	69.0
5	6.25	Wingless	75.5	68.8
6	6.25	Wingless	76.8	70.3

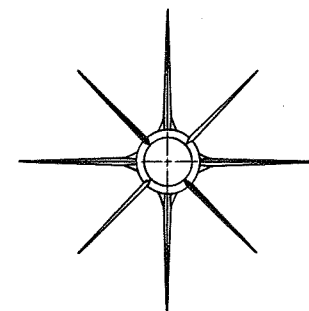
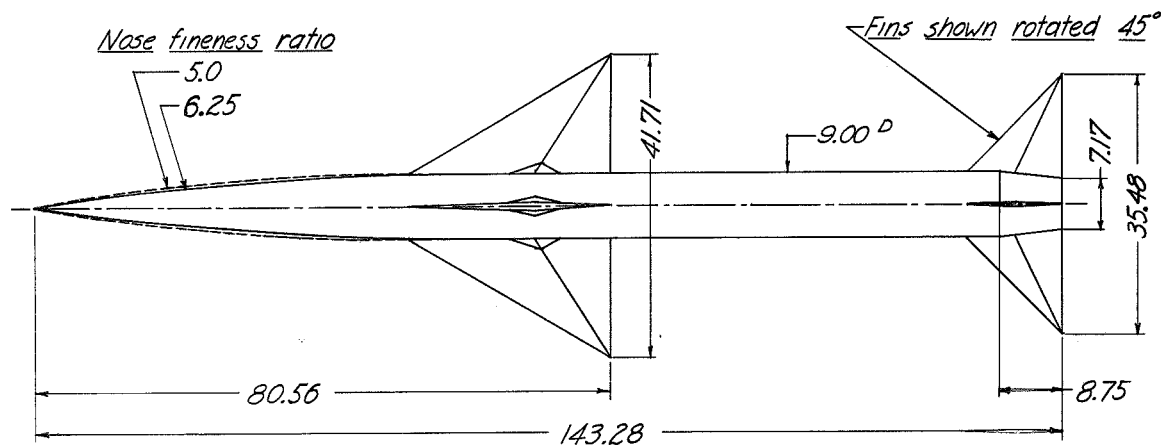


TABLE II

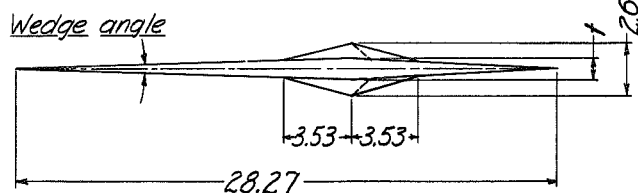
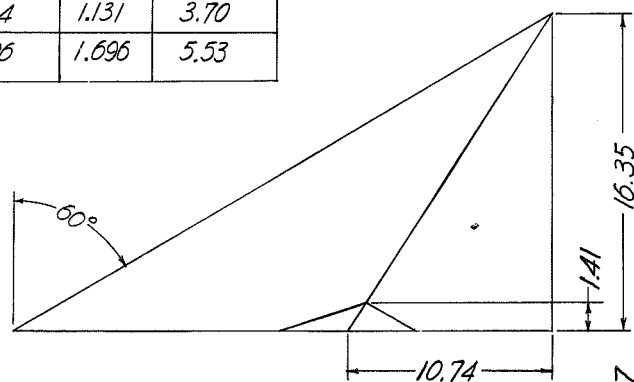
NOSE COORDINATES

Fuselage radius (in.)	Fuselage station (in.)	
	Nose fineness ratio = 5.00	Nose fineness ratio = 6.25
0	0	0
.066	.113	.141
.110	.225	.281
.185	.450	.563
.251	.675	.844
.367	1.125	1.406
.472	1.575	1.969
.615	2.250	2.813
.789	3.150	3.938
1.027	4.500	5.625
1.226	5.738	7.172
1.698	9.000	11.250
2.260	13.500	16.875
2.513	15.750	19.688
2.750	18.000	22.500
2.973	20.250	25.313
3.182	22.500	28.125
3.378	24.750	30.938
3.562	27.000	33.750
3.632	27.900	34.875
3.733	29.250	36.563
3.891	31.500	39.375
4.167	36.000	45.000
4.381	40.500	50.625
4.500	45.000	56.250

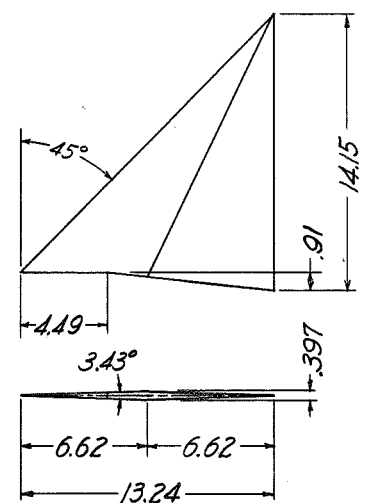
NACA



Wing thickness ratio	t	Wedge angle (deg)
0.04	1.131	3.70
.06	1.696	5.53



Wing detail



Fin detail



Figure 1.- General arrangement of test vehicles. All dimensions in inches.

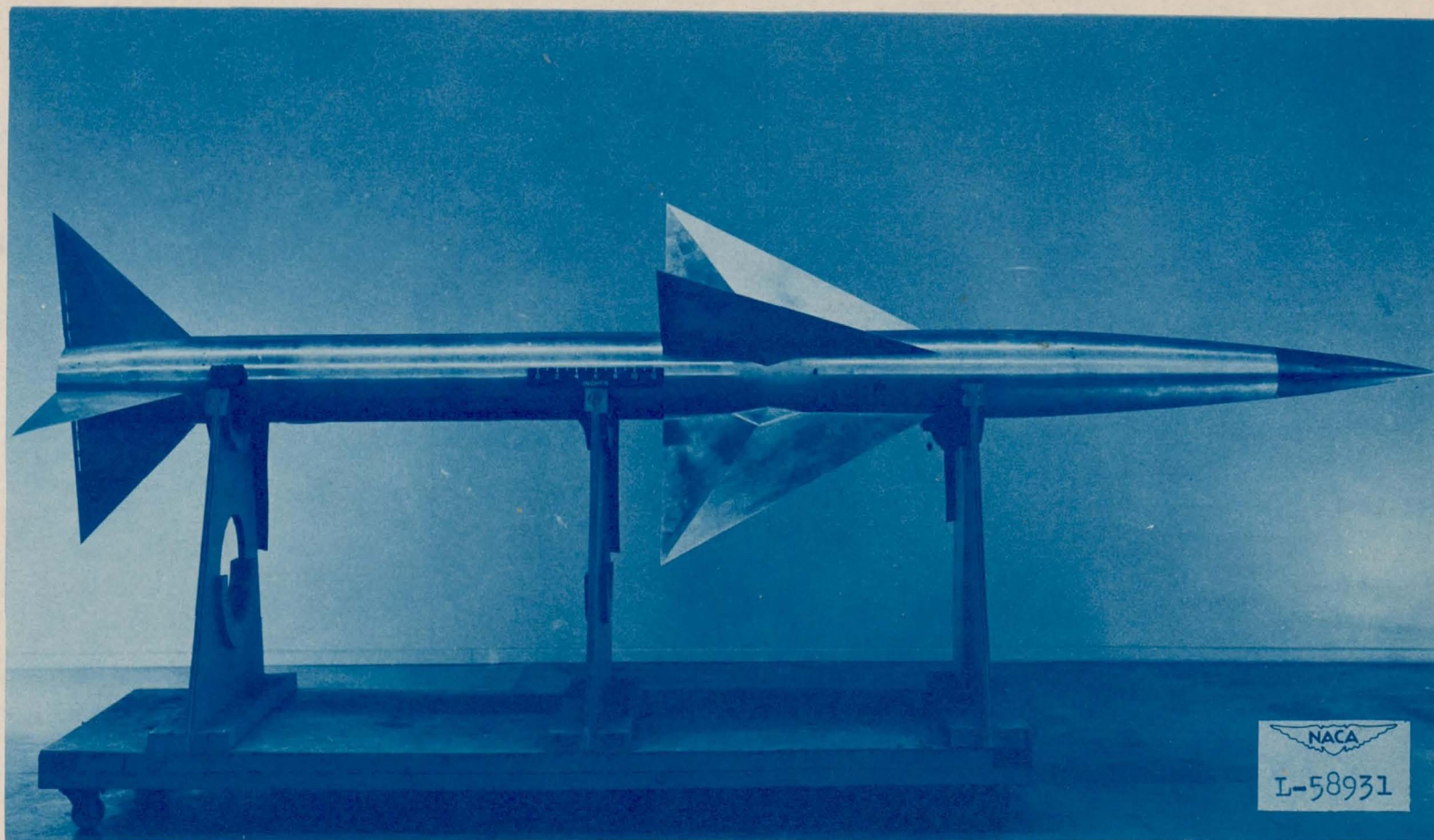


Figure 2.- A typical XAAM-N-2 model. Nose fineness ratio, 5.00; wing thickness ratio, 0.04.

CONFIDENTIAL

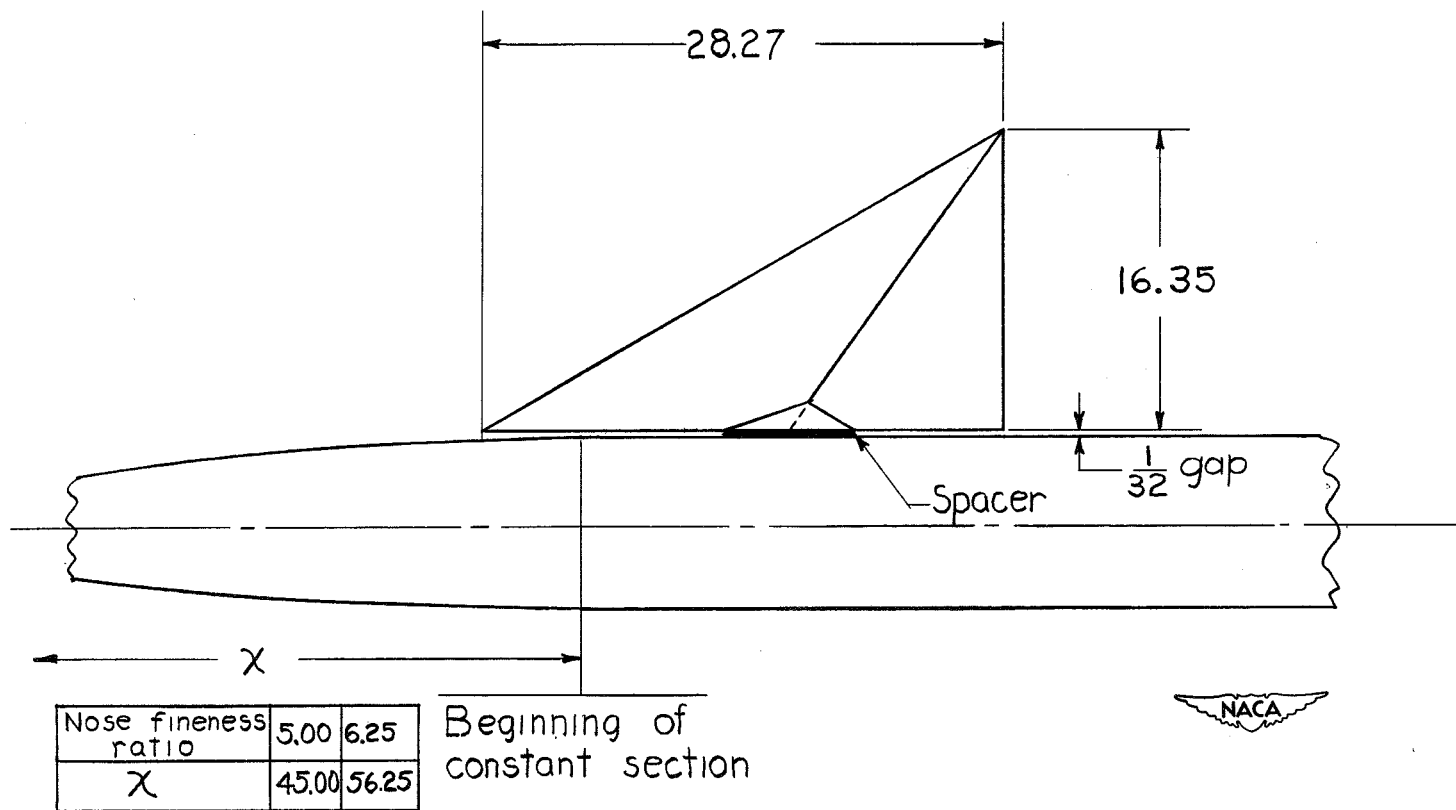


Figure 3.- Wing-fuselage juncture. All dimensions in inches.

CONFIDENTIAL

NACA RM SL50C16a

CONFIDENTIAL

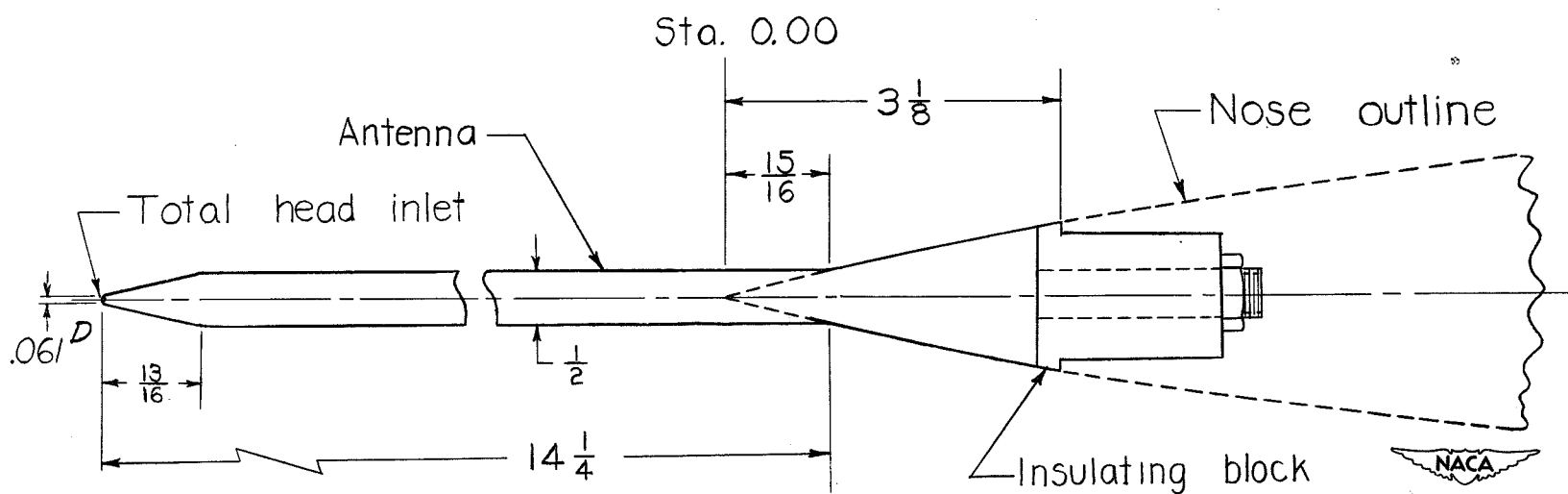
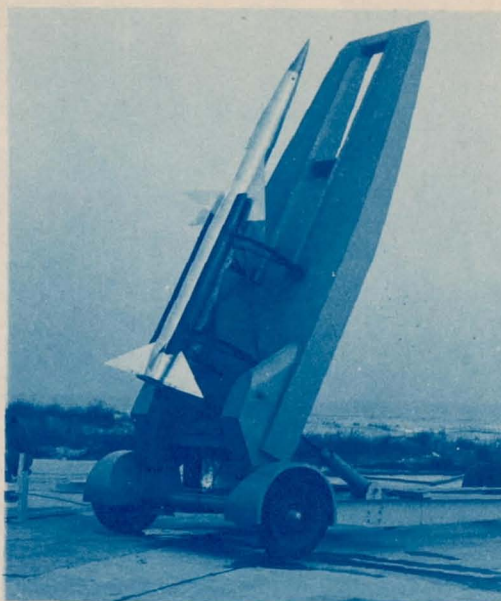


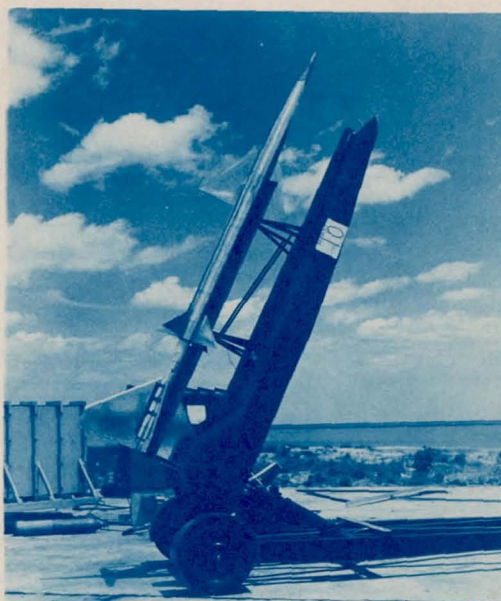
Figure 4.- Nose antenna details. All dimensions in inches.

CONFIDENTIAL



NACA
L-58886

Figure 5.- Unboosted XAAM-N-2 model on launcher.



NACA
L-61240

Figure 6.- Boosted XAAM-N-2 model on launcher.

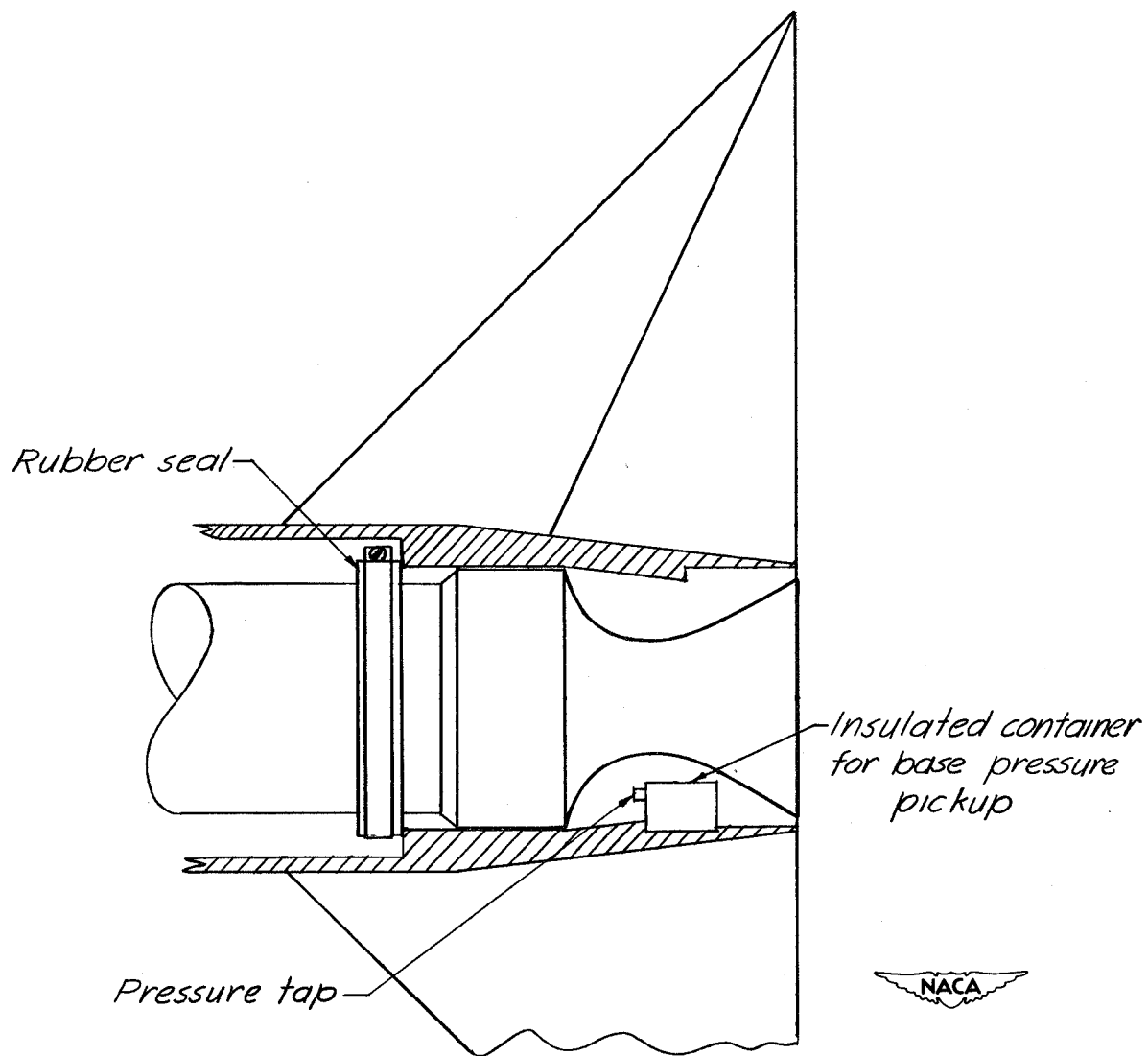


Figure 7.- Sketch of base-pressure pickup installation.

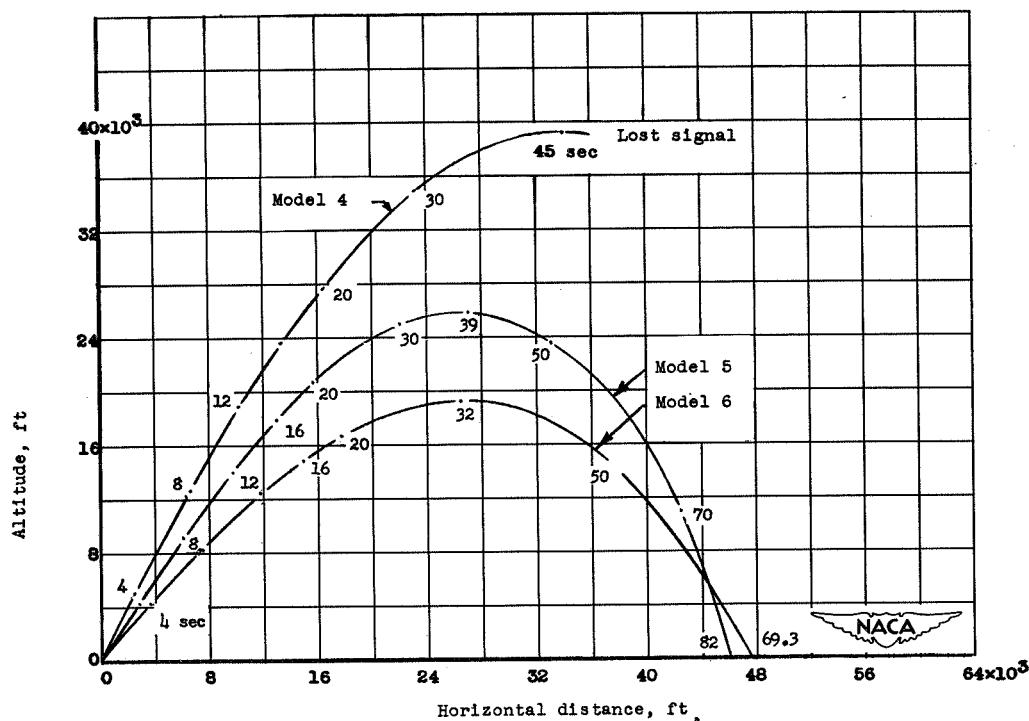


Figure 8.- Typical flight paths obtained with SCR 584 radar set.
Numbers refer to time after firing.

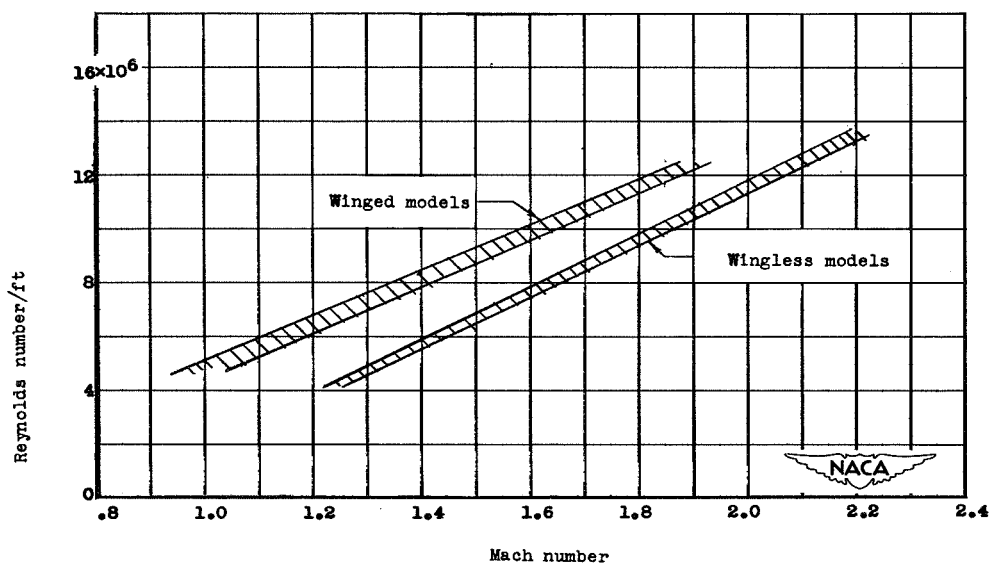
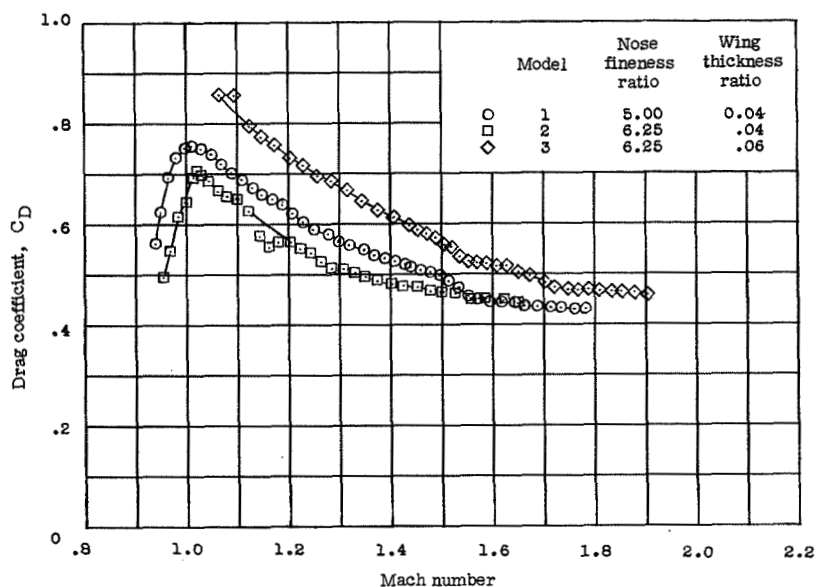
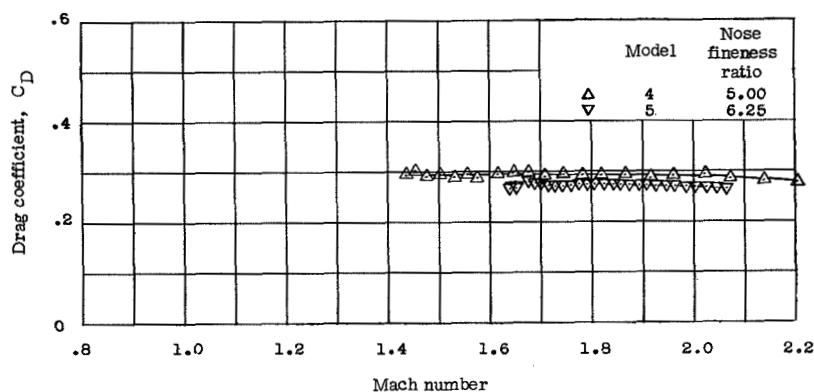


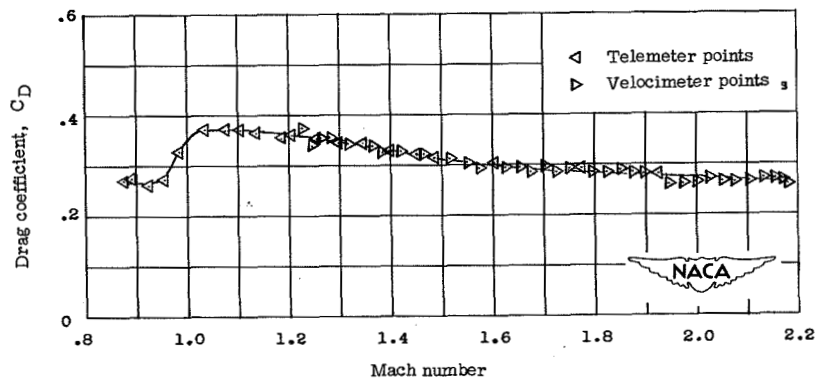
Figure 9.- Variation of Reynolds number with Mach number for range of test conditions.



(a) Winged models, velocimeter data points.



(b) Wingless models, velocimeter data points.



(c) Wingless model 6; nose fineness ratio, 6.25.

Figure 10.- Typical drag-coefficient-data points.

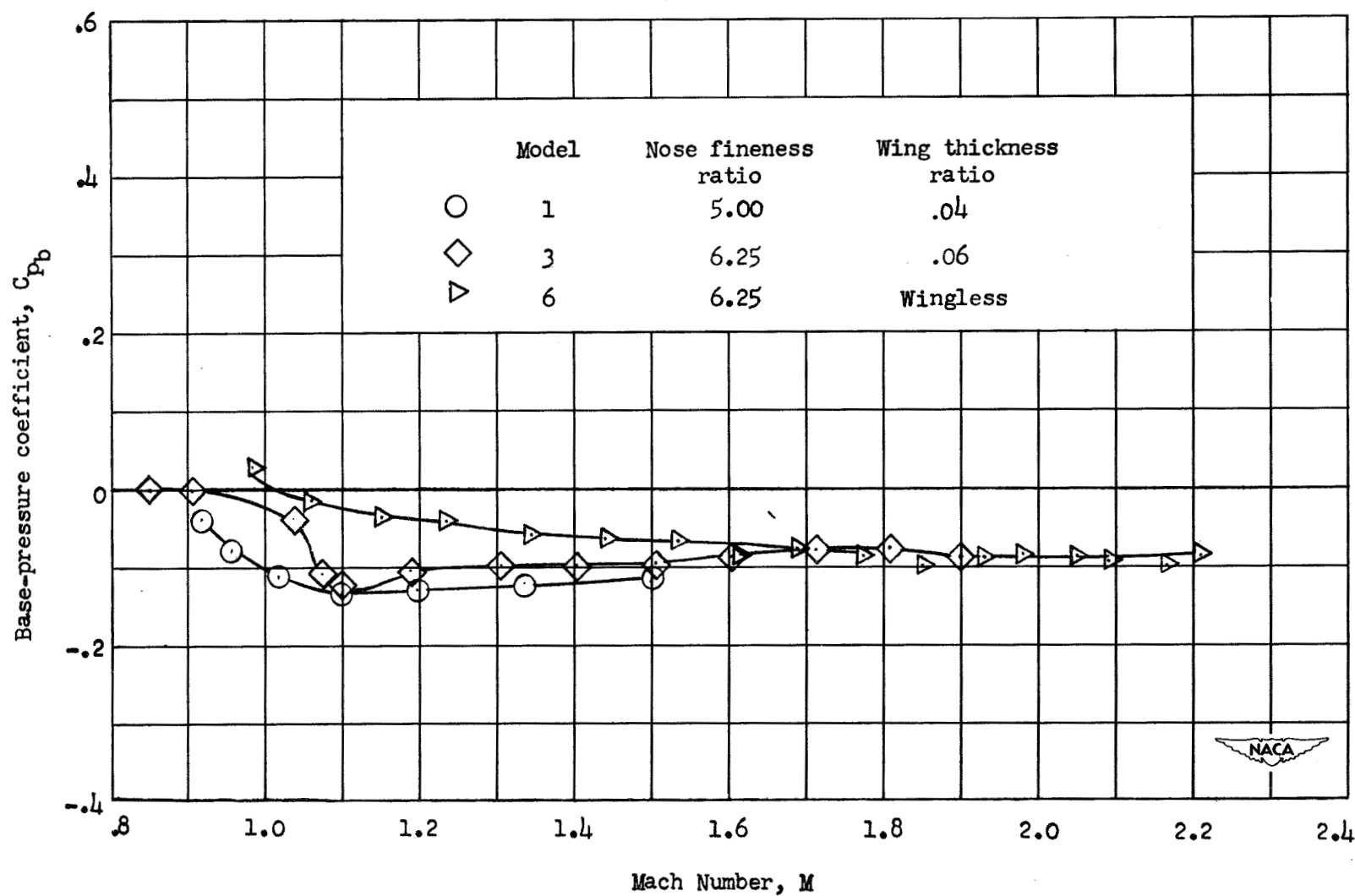


Figure 11.- Variation of base-pressure coefficient with Mach number.

CONFIDENTIAL

NACA RM SL50C16a

CONFIDENTIAL

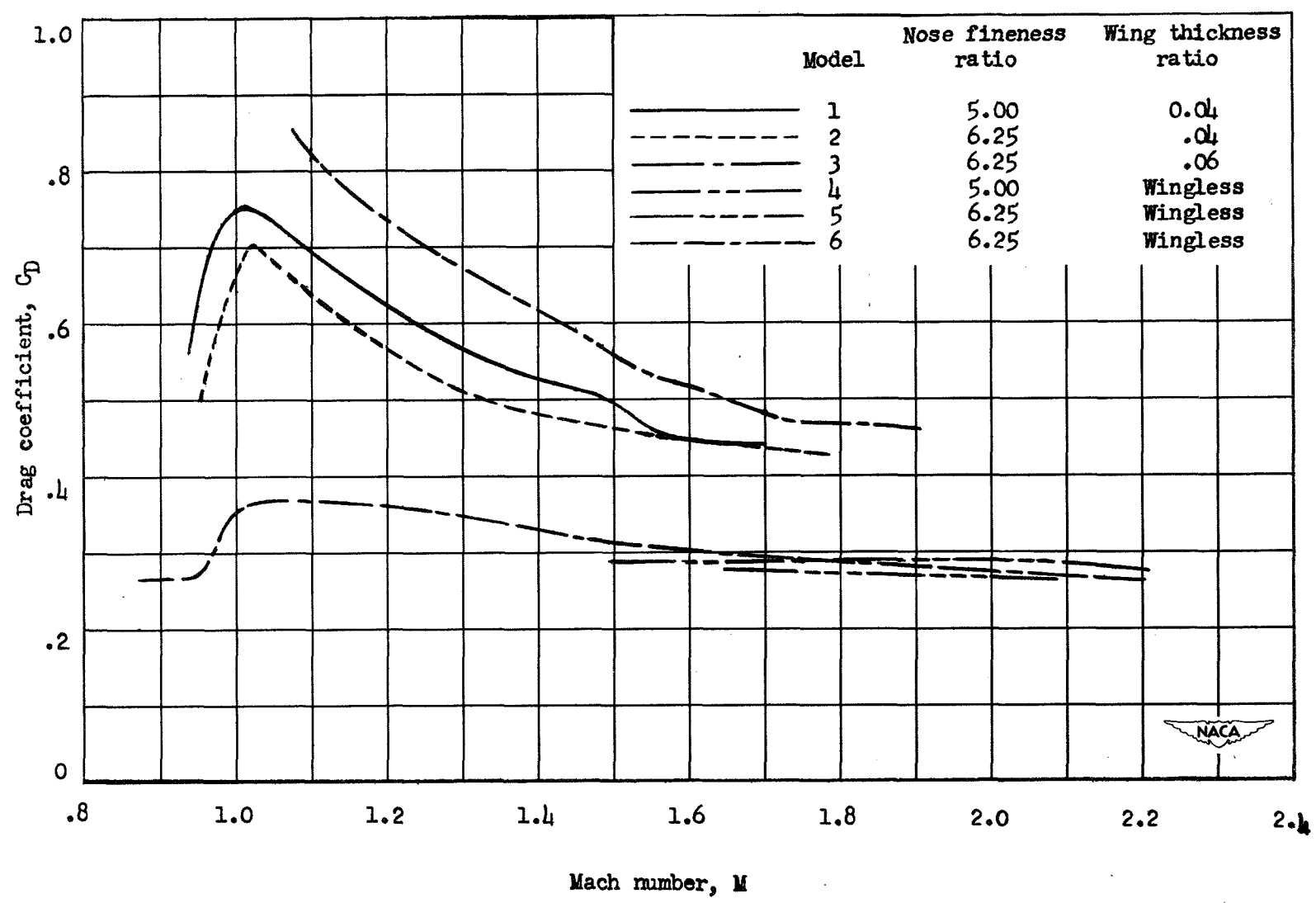


Figure 12.- Variation of drag coefficient with Mach number.

CONFIDENTIAL

012010

NACA RM SL50C16a

CO

Restriction/
Classification
Cancelled

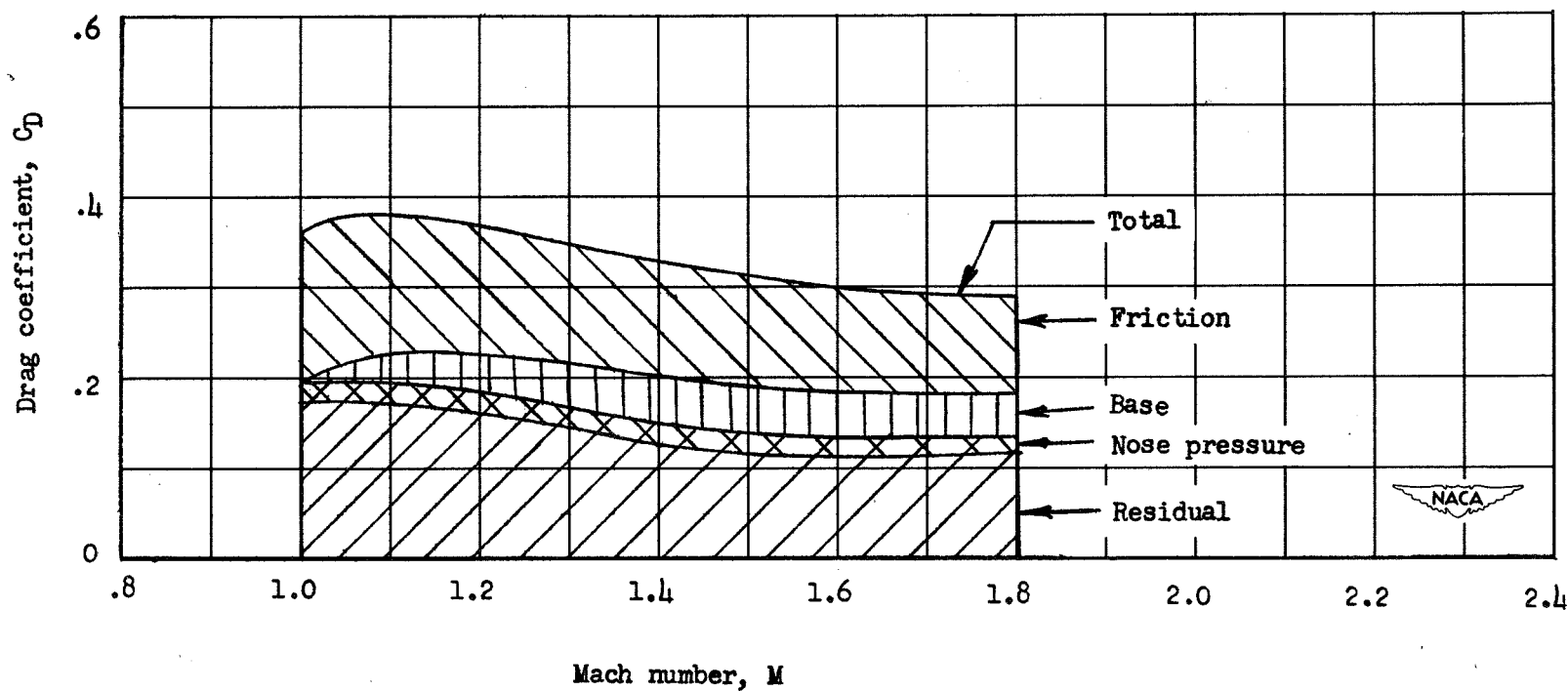


Figure 13.- Component drag of wingless model 6.

Restriction/Classification Cancelled

CONFIDENTIAL